2025 EAGE ANNUAL
86TH CONFERENCE & EXHIBITION
TOULOUSE | FRANCE

Multi-dimensional deconvolution as a framework for processing and targeted imaging - a comparison of redatuming approaches

Ivan Vasconcelos, Shearwater GeoServices;
Ning Wang, KAUST;
Matteo Ravasi, presently Shearwater GeoServices, formerly KAUST;
Chris Purcell, Shearwater GeoServices.

Across many applications in seismic processing and imaging, multi-dimensional deconvolution (MDD) appears in many forms, and over recent years, has gained much traction, particularly in the context of processing ocean bottom (OB) data. Leveraging a computational implementation that combines matrix-free time-domain multi-dimensional convolutional operators with efficient numerical optimisation schemes, we approach MDD as a general framework applicable to multiple geophysical purposes. As examples in the context of processing OB data, here we discuss and compare receiver-side MDD and source-side MDD: The former redatums the survey to the receiver datum, while the latter redatums it to the source surface – both without free-surface effects. For reservoir imaging and monitoring, we discuss target-oriented redatuming (TOR) by MDD, which in turns relies on input wavefields resulting from a prior redatuming step, such as wavefield injection or Marchenko-based approaches. Using OB data from the Volve field, we compare source- and receiver-side MDD as alternatives to processing OB data, where we observe both of the surface-based approaches yield good-quality, comparable results in estimating responses and corresponding depth images without free-surface effects, with the source-side method showing increased robustness to increased receiver spacing. When comparing depth imaging results, we observe that TOR by MDD also delivers comparable images to either surface-based methods, reassuring us that such targeted imaging and monitoring approaches are viable for our MDD framework.

Multi-dimensional deconvolution as a framework for processing and targeted imaging - a comparison of redatuming approaches

Introduction

Recently, and in particular in the context of processing ocean-bottom (OB) seismic data, multi-dimensional deconvolution (MDD) has received much interest from the geophysical community, and has greatly evolved its earlier concepts (Amundsen, 2001), to current, more sophisticated practice (e.g., Boiero et al., 2023, Poole et al., 2024). In line with these advances, our study builds on a generalisation of time-domain MDD (Vargas et al., 2021), which is framed within a general-purpose, operator-based inversion framework that can be applied not only for OB data processing at scale (Ravasi & Vasconcelos, 2025), but also in the context of target-oriented imaging and monitoring (e.g., Vasconcelos et al., 2024) when combined with state-of-the-art wavefield redatuming techniques (Wang & Ravasi, 2024). Here, we review how our implementation of time-domain MDD lends itself to multiple applications by looking at three separate approaches that rely on MDD while directly comparing them in the context of Volve field data.

The MDD framework – from OBN processing to Target-oriented Redatuming

Generally, solving the MDD problem in the time-domain reduces to solving a linear inverse problem of the form (Vargas et al., 2021, Vasconcelos et al., 2024):

$$\min_{\mathbf{m}} \|\mathbf{U} - \mathbf{Q}\,\mathbf{X}\,\mathbf{M}\|_2^2 + \lambda\|\mathbf{C}\mathbf{M}\|_2^2 \qquad (1)$$

where $\mathbf{X}\,\mathbf{M} = \mathbf{R}^T$ is a desired reflectivity response, preconditioned with physical hard-constraints embedded within $\mathbf{X}$, imposing, e.g., causality, reciprocity (Vargas et al, 2021) or regularized with soft-constrains by $\mathbf{C}$ e.g., directional smoothing (Ravasi & Vasconcelos, 2025). To think of MDD as a framework is to simply recognise that input-data-related $\mathbf{U}$ and data-operator $\mathbf{Q}$ fields are problem-dependent, i.e., they can be chosen for a variety of processing scenarios or for applications in imaging-related redatuming – next we present specific instances of such choices.

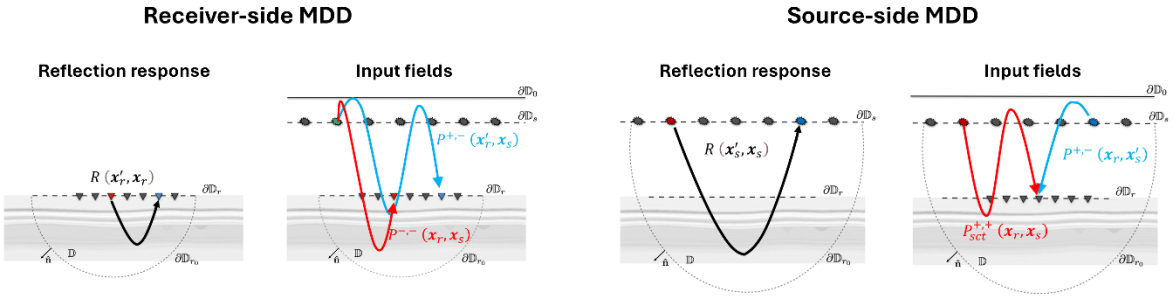

Figure 1 *Schematic representation of the physical setups for either receiver- (left-hand panels) or source-side MDD. The receiver-side setup relies on up- and down-going fields impinging on the receiver datum, while the source-side uses a decomposition of the receiver-side down-going wavefield into up (source ghost)- and down (downwards emission) fields on the source datum. Both setups are devoid of free-surface effects in the retrieved reflection responses, however, the source-side setup retains wavepaths through the water column.*

First, we consider the application of MDD for processing ocean-bottom (OB) data (be it node- or cable-based). The traditional approach to MDD for OB is the so-called receiver-side MDD, because it relies on the well-known physical relation (e.g., Wapenaar et al., 2011; Vargas et al., 2021) where the relationship between an overburden-free reflectivity response, and associated up- and downgoing fields is given by

$$P^-(\boldsymbol{x}_r, \boldsymbol{x}_s) = \int_{\partial\mathbb{D}_r} R\left(\boldsymbol{x}_r', \boldsymbol{x}_r\right) * P^+(\boldsymbol{x}_r', \boldsymbol{x}_s)\, d\boldsymbol{x}_r' \quad , \quad \mathbf{P}^- = \mathbf{R}\mathbf{P}^+ ; \qquad (2)$$

where $*$ denotes time-domain convolution, and P^-, P^+ and R are the time-domain fields associated with the upgoing, downgoing and target Green's functions at the receiver datum coordinates depicted in Fig. 1 – after MDD, this yields a reflectivity response with sources and receivers redatumed to the receiver datum. In the case of OB data processing, the fields P^+ and P^- are observed data (after pre-processing), however, in the case of TOR for reservoir imaging (see below), these are instead P^+_{red} and P^-_{red}, i.e., up- and down-going fields at depth resulting from a prior redatuming step (Vasconcelos et al., 2024; Wang & Ravasi, 2024). In Eq. 2 we consider fields without source-side separation (de-ghosting), though in practice we use source-separated fields for Receiver-side MDD (see below).

A less conventional alternative to treating OB data, leading to the source-side MDD setup, is to rely instead on the following integral relation (Almagro Vidal et al., 2014; Wang & Ravasi, 2024):

$$P^{+,+}_{sct}(\boldsymbol{x}_r, \boldsymbol{x}_s) = \int_{\partial \mathbb{D}_s} R(\boldsymbol{x}'_s, \boldsymbol{x}_s) * P^{+,-}(\boldsymbol{x}_r, \boldsymbol{x}'_s)\, d\boldsymbol{x}'_s \quad , \quad \left[\mathbf{P}^{+,+}_{sct}\right]^T = \mathbf{R}[\mathbf{P}^{+,-}]^T ; \tag{3}$$

where the transpose indicates the integration over source instead of receiver coordinates (see Eq. (2)), and now both $P^{+,+}_{sct}$, $P^{+,-}$ are down-going-only on the receiver-side, with the former being down-going (downward emission) and the latter up-going (source ghost) on the source datum (right side of Fig.1). The field $P^{+,+}_{sct}$ denotes the field $P^{+,+}$ after the removal of direct arrivals (Almagro Vidal et al., 2014; Wang & Ravasi, 2024). In this source-side setup, the response R corresponds to the medium's full Reflectivity redatumed to the acquisition source datum.

Thus, in this study, our choices for input-data-related $\mathbf{U}$ and data-operator $\mathbf{Q}$ from Eq. (1) are:

- *Receiver-side MDD*: $\mathbf{U} = [\mathbf{P}^{-,-}]^T$, and $\mathbf{Q} = [\mathbf{P}^{+,-}]^T$. This means we maintain the receiver dimension as the integration dimension as in Eq. (2), but on the source-side we choose to use source separated (i.e., de-ghosted) data consisting of up-going waves at emission points (i.e,, the upwards-emitted ghost) – this is to maintain full consistency between the operators (and thus results) from both receiver- and source-side MDD. This choice does not change the physical meaning of the retrieved Reflectivity (left-hand side of Fig. 1);
- *Source-side MDD*: $\mathbf{U} = \left[\mathbf{P}^{+,+}_{sct}\right]$ and $\mathbf{Q} = [\mathbf{P}^{+,-}]$. This is in line with the source-side integration and wavefields as per Eq (3) and the right-hand side of Fig. 1.
- *TOR by MDD:* $\mathbf{U} = [\mathbf{P}^-_{red}]^T$ and $\mathbf{Q} = [\mathbf{P}^+_{red}]^T$. This choice denotes operator integration over the (virtual) receiver datum. Here, we use depth-domain fields redatumed by means of the Upside-down Rayleigh-Marchenko approach of Wang & Ravasi (2024) – this choice is also fully consistent with the above, in that the input fields for this Marchenko approach are the exact same as used for the source- and receiver-MDD applications.

Finally, we note all **Q**s are implemented as implicit, matrix-free operators enabling large-scale time-domain optimisation (e.g., Vargas et al., 2021; Ravasi & Vasconcelos, 2025). We rely on the LSQR solver for all examples herein and employ the causality and reciprocity preconditioners after Vargas et al. (2021).

Volve field data testing

For all of our tests, we use one OBC receiver line of the Volve field data, together with the closest possible source line so as to mimic a 2D dataset. The data consist of 240 discrete sources (approx. 50 m spacing) and 240 receivers (approx. 25 m spacing), with apertures as shown in Fig. 3a. Pre-processing steps consist of bandpassing (preserving the unaliased part of the data - up to 30Hz), up/down separation at the OB receivers and source-side de-ghosting. This yields the input fields for Receiver- and Source-side MDD tests as above. For TOR by MDD, we apply the Marchenko-based redatuming of Wang & Ravasi (2024) to obtain up- and down-going fields at a 1990m depth datum, extending from 4000-8000 m lateral distance (Fig. 3a), with virtual sources and receivers sampled at 25 m intervals.

We begin by inspecting shot gathers from estimated reflectivity responses in Fig. 2. Firstly, here, we observe that the responses from each setup yield gathers with varying offset ranges, due to the fact that each MDD setup corresponds to datums with varying lateral apertures (Fig. 3a) – noting, in particular,

that the Source-side MDD response has the widest aperture due to the acquisition geometry. While the fully-receiver-sampled receiver- and source-side MDD responses are comparable in quality, the TOR by MDD result shows lower S/N though still retrieving identifiable events – this is because TOR operates on Marchenko-redatumed inputs, which are themselves noisier than the OB input data.

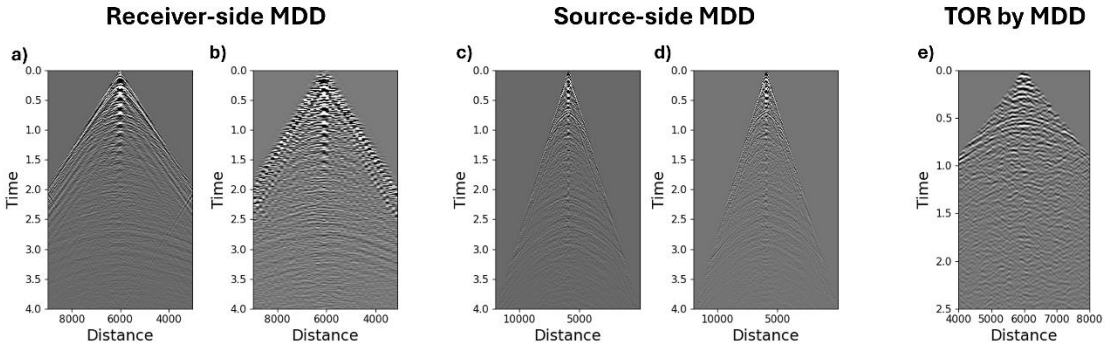

Figure 2 *Volve field data gathers retrieved from various MDD setups. All gathers shown correspond to selecting a shot-gather from each reflectivity response for a virtual source location at the center of each corresponding datum (see Fig. 3a). We show retrieved responses using the full sampling of OB receivers for both receiver-side (a) and source-side (c) MDD, as well as their counterpart responses after sub-sampling the receivers by a factor of 5 (panels b and d). Panel e) shows the response from Target-Oriented Redatuming (TOR) by MDD, using subsurface fields estimated by Marchenko redatuming (Wang & Ravasi, 2024).*

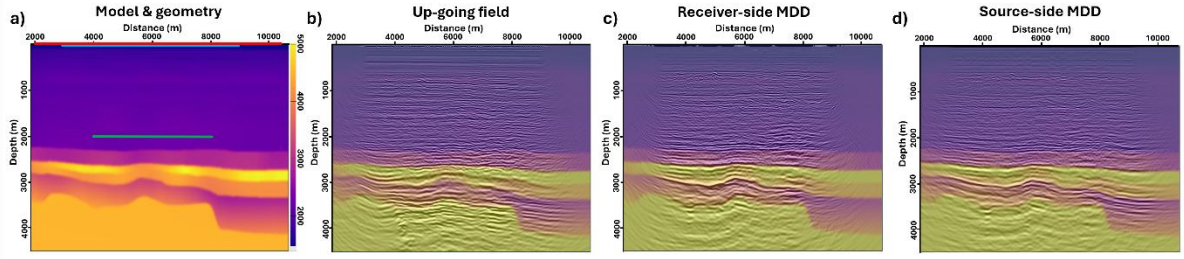

Figure 3 *Volve model, acquisition geometry and RTM images from MDD setups. Panel a) is the velocity model (colour bar in m/s). Panels b-d) display RTM images overlaid on the velocity model (from left to right, respectively): using the up-going fields from the original acquisition, from the receiver datum (receiver-side MDD), and from the source datum (source-side MDD). Panel a) displays the location and aperture of the source (red), receiver (light blue) and TOR (green) datums.*

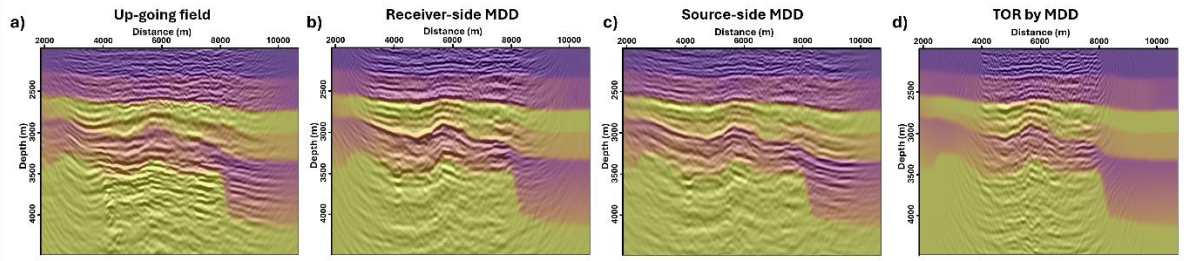

Figure 4 *Comparison of RTM images below the TOR chosen depth datum at 1990m depth. Panels a-c) are zoomed-in on the corresponding RTM images in Fig. 3, whereas panel d) is the RTM image from the TOR virtual response retrieved at the 1990m-depth datum, laterally extending from 4000-8000m.*

Additionally, in Fig. 2, we show source- and receiver-side MDD estimates after sub-sampling the OB receiver data to 125 m – i.e., mimicking the effect of larger receiver gaps common in OB acquisition. We observe that the source-side MDD result remains notably more robust to the larger receiver spacing than that from the conventional receiver-side approach: this is because larger receiver spacing subsamples the underlying operator in the receiver-side case (see Eq. 2), while the source-side operator

remains equally dense and only the number of equations to solve the inverse problem reduces in light of larger receiver spacing.

To better assess how these various MDD approaches ultimately affect depth images, in Figs. 3 and 4 we show RTM images for the full model and below the target datum, respectively. In both these Figures, we compare MDD-derived images with RTM of the up-going only field, i.e., the $\mathbf{U} = [\mathbf{P}^{-,+}]^T$ used in the Receiver-side MDD. Very encouragingly, the first observation is that all MDD retrieve highly structurally-consistent images, and all achieve a significant uplift in terms of expected suppression of free-surface effects when compared to the up-going-only image. The images from MDD-derived data yields different lateral apertures - with the source-side being the widest and the TOR one the narrowest. This is expected given that in each case all sources and receivers used in imaging lie within either the source, receiver or TOR datums seen in Fig 3a. Specifically, when considering Fig. 4d, we see that the TOR-based reflectivity leads to an image of acceptable quality, but unlike the images in 4b or 4c, it does not require any propagation through/knowledge of the overburden for imaging – thus affirming its value for targeted reservoir imaging and monitoring.

Conclusion

Using Volve field data as an example, we demonstrate how a flexible MDD framework can be applied to generate multiple data sets either in, e.g., the context of OB data processing or target-oriented reservoir imaging and monitoring, among several other potential scenarios. In the case of OB data processing, we compare the more conventional receiver-side MDD approach to source-side MDD, with the latter showing greater robustness to larger receiver spatial sampling while also resulting in images of wider lateral aperture – this comes at the cost of more expensive MDD calculations given the notably larger operators in source-side MDD for sparse receiver scenarios. In the context of target-oriented reservoir imaging and monitoring, we demonstrate that imaging depth-domain data from TOR by MDD achieves images of comparable quality to surface-based ones, even though the TOR-retrieved data has lower S/N compared to MDD estimates from observed data, as a result of the previous step of Marchenko-based redatuming. While realising the full potential of time-domain MDD on large 3D data at scale is a computational endeavour still the subject of research, our results support the promise of time-domain MDD as a stable and reliable framework capable of addressing current challenges in seismic processing and in advanced reservoir imaging and monitoring.

Acknowledgements

We thank Paolo Terenghi, Arash JafarGandomi and Lorenzo Casasanta (all Shearwater GeoServices) for valuable discussions and input. We acknowledge Shearwater GeoServices for permission to publish this study.

References

[1] Amundsen, L. [2001] Elimination of free-surface related multiples without need of a source wavelet: Geophysics, 66, 327–341.
[2] Almagro-Vidal, C., Wapenaar, K. [2014] Passive seismic interferometry by multi-dimensional deconvolution-decorrelation. SEG Technical Program Expanded, doi: https://doi.org/10.1190/segam2014-1208.1
[3] Boiero, D., Mahat, S., Bagaini, C., and Ortin, M. [2023] True-amplitude multiple prediction in sparse ocean-bottom acquisitions using a multidimensional deconvolution approach: 84th EAGE Annual Conference & Exhibition.
[4] Poole, G., Haacke, R., and King, S. [2024] Sparse Time-Domain Multi-Dimensional Deconvolution for OBN Data: 85th EAGE Annual Conference & Exhibition.
[5] Ravasi, M. and Vasconcelos, I. [2025] Regularising time-domain multi-dimensional deconvolution with offset-directional derivatives. Submitted to the 85th EAGE Annual Conference & Exhibition.
[6] Vargas, D., Vasconcelos, I., Ravasi, M., and Luiken, N. [2021] Time-domain multidimensional deconvolution: A physically reliable and stable preconditioned implementation. Remote Sensing, 13, 3683.
[7] Vasconcelos, I., Vargas, D., Ravasi, M. and Terenghi, P. [2024] Deblurring-based, time-domain multi-dimensional deconvolution – redatuming for target-oriented imaging. 85th EAGE Annual Conference & Exhibition.
[8] Wang, N., and Ravasi, M. [2024] Upside-down Rayleigh-Marchenko: A practical redatuming scheme for seabed seismic acquisitions. Geophysics, 89, https://doi.org/10.1190/geo2023-0743.1.